# Parametric instabilities of intense lasers from interaction with relativistic hot plasmas

Z.-M. Sheng,[1] K. Mima,[1] Y. Sentoku,[2] and K. Nishihara[1]
[1]*Institute of Laser Engineering, Osaka University, 2-6 Yamada-oka, Suita, Osaka 565-0871, Japan*
[2]*Institute of Laser Technology, 2-6 Yamada-oka, Suita, Osaka 565-0871, Japan*
(Received 31 August 1999; revised manuscript received 22 November 1999)

The stimulated Raman scattering (SRS) and relativistic modulational instability (RMI) of intense lasers in relativistic hot plasmas are studied, using the waterbag distribution in momentum space. Two cases are considered: a single hot electron distribution and a cold plasma attached with a hot electron tail. It is shown that both high temperatures and hot electron tails can significantly reduce the instability growth rates, shift the unstable regions in the wave-vector space, and change the Raman scattering frequency spectra from the cold plasma theory. In particular, at low-light intensities, there exists a cutoff thermal velocity beyond which SRS is completely suppressed. At high-light intensities, no clear cutoff thermal velocity is found owing to the merging of SRS with RMI.

PACS number(s): 52.40.Nk, 52.35.Mw, 52.60.+h, 52.65.Rr

## I. INTRODUCTION

Recently there has been considerable interest in parametric instabilities in plasmas in the regime where the driving lasers are at relativistic high intensities ($I \geqslant 10^{18}$ W/cm$^2$), now available owing to recent advance in the laser technology. With these kinds of lasers normally having a duration less than 1 ps, the electron parametric instabilities are more important than those concerned with ion motion. In comparison with earlier theories for relatively low-light intensities [1,2], new features of the electron parametric instabilities are found in the relativistic intensity regime. They are characterized by the broadening of unstable regions in the wave vector space and merging of the unstable regions of different instabilities, high temporal growth rate up to a fraction of the laser frequency, spatial-temporal behavior due to the short pulse duration, strong harmonics generation, and new instability excitation, such as the relativistic modulational/filamentation instability, etc. [3–11]. In most of these works, plasma electrons are assumed to be cold without drift motion. However, now there is growing evidence showing that this assumption is generally not satisfied in laser-plasma interaction involving relativistic intense lasers.

Partially motivated by the concept of the fast ignitor [12], considerable studies, either with particle-in-cell (PIC) codes [13–18] or in experiments [19–23], are devoted to the issues of propagation of short pulse intense lasers in underdense plasma and hole boring through overdense plasma. One of the main pictures is that a large amount of electrons are accelerated to very high energy by lasers together with induced electric and magnetic fields in plasma. These electrons form current jets moving in the forward direction inside the self-focusing channels or individual filaments of the light beams. Meanwhile return currents flow in the opposite direction in the surrounding regions. Such electron current pipes are accompanied by the self-focusing of the laser beams, the self pinching of the inner currents or current jets, and strong magnetic field generation. In addition to the forward acceleration, some PIC simulations also demonstrated that electrons inside the channels are heated randomly to extremely high temperatures [14–16]. The high-energy density of electrons inside the channels suppresses the electron blowout or cavitation by the ponderomotive force in the transverse direction [16]. In view of these observations, a new theory on parametric instabilities is necessary to account for the effects of the drift motion and the high temperatures of electrons. The drift motion and high temperatures can significantly change the growth rates and the frequency spectra of the parametric instabilities, and as a result, affect the behavior of laser pulse propagation in underdense plasma regions. In fact, some primary study [24] and a one-dimensional PIC simulation already show the suppression of the instabilities by high temperatures [5].

In this paper, we study both the stimulated Raman scattering (SRS) and the relativistic modulational instability (RMI) of intense lasers in plasma with either high electron temperatures or drifting velocities, thereby extend previous one-dimensional theories on relativistic parametric instabilities in cold plasmas [3–5]. One of the main points is that a relativistic waterbag model in electron momentum space is adopted, which allows for considerable simplification of the final dispersion relation. One can even use several Heaviside functions to approximate the real distribution including possible high-energy tails. The resulting dispersion relation is a polynomial, which can be solved numerically. The outline of this paper is as follows. In Sec. II, a one-dimensional dispersion relation valid for relativistic high-electron temperatures is described. In Sec. III, a symmetric waterbag distribution about zero momentum is used to study the dependence of SRS and RMI on electron temperatures and plasma densities. For the relevance to the fast ignitor simulations mentioned above, in Sec. IV, SRS and RMI are studied for electrons distributed with two different temperatures, a cold component described by the delta function at zero momentum and a hot-tail component with momenta extending from zero to some high momentum. A summary and discussions of the results are given in Sec. V.

## II. DISPERSION RELATION

We consider a laser pulse propagating in homogeneous plasma. It is circularly polarized with the vector potential $\mathbf{a}_0=(a_0/2)[\mathbf{e}_0 \exp(ik_0x-i\omega_0t)+\text{c.c.}]$ normalized by $mc^2/e$ with $\mathbf{e}_0=(\mathbf{e}_y \pm i\mathbf{e}_z)/\sqrt{2}$ and $a_0$ a real constant. There is a dispersion relation for this laser pulse

 

$$\omega_0^2 = k_0^2 c^2 + \omega_p^2 \int dp f(p)/\gamma, \tag{1}$$

where $\omega_p^2 = 4\pi N_0 e^2/m$ is the electron plasma frequency, $f(p)$ is the electron distribution function normalized by the electron density $N_0$, $p$ is the electron momentum normalized by $mc$, and $\gamma = (1 + a_0^2/2 + p^2)^{1/2}$ is the relativistic factor. The dispersion relation (1) is purely electromagnetic and is valid even if the plasma electrons involve net drift motion, as shown in the Appendix. If there is a net current, for example, inside a self-focusing channel of a laser beam, there arises a self-generated quasistatic magnetic field. In the following study in one-dimensional geometry, this static magnetic field will be neglected. This is justified if the plasma is less than a certain width $W$. Noting that the cyclotron frequency of electrons in the self-generated magnetic field has a maximum value in the edge of the plasma, thus the effect of the magnetic field can be ignored if the maximum cyclotron frequency $\omega_c = (W/2c)(\omega_p^2/\gamma_0)(v_0/c) \ll \mathrm{Min}\{\omega_p/\gamma_0^{1/2}, \omega_0\}$, where $v_0$ is the average drifting velocity of electrons. Since $\omega_p/\gamma_0^{1/2} < \omega_0$, one obtains $W < (c/v_0) W_A$ with $W_A = 2c\gamma_0^{1/2}/\omega_p$ the Alfvén radius. The Alvén radius is defined by $W_A = (I_A/\pi e n_0 v_0)^{1/2}$ with the Alfvén current $I_A = (mc^3/e)(\gamma_0 v_0/c) \approx 17(\gamma_0 v_0/c)$ kA. Normally $W \gg \lambda_0$ with $\lambda_0$ the laser wavelength, we then obtain the condition to neglect the magnetic field: $\omega_p^2/\gamma_0 \omega_0^2 \ll 1/\pi(v_0/c)^2$. In the one-dimensional case and ignoring the magnetic field, it has been shown, starting with the Vlasov equation for electrons, that the dispersion relation for parametric instabilities can be written as [5]

$$D_{+1} D_{-1} - (D_{+1} + D_{-1}) S = 0, \tag{2}$$

where $D_{\pm 1} = \omega^2 - c^2 k^2 \pm 2(\omega\omega_0 - c^2 k k_0)$ with $\omega$ and $k$ the frequency and wave vector of the involved plasma wave, and the coupling function

$$S = \frac{a_0^2 \omega_p^2}{4} \left\{ \frac{\omega_p^2}{c^2 k^2 \epsilon} \left[ \int \frac{dp\, \partial f(p)/\partial p}{\gamma (v - \omega/ck)} \right]^2 + \int \frac{dp\, \partial f(p)/\partial p}{\gamma^2 (v - \omega/ck)} - \int \frac{dp f(p)}{\gamma^3} \right\}, \tag{3}$$

with the dielectric function $\epsilon = 1 - (\omega_p^2/c^2 k^2) \int dp\, \partial f/\partial p (v - \omega/ck)^{-1}$ and the velocity $v = p/\gamma$. Equation (2) is actually the result of four-wave interactions. It can be obtained alternatively by considering the distribution function of electrons as an assembly of cold electron beams with different velocities. From this point of view, the dispersion relation can be derived in a similar way as for a cold beam, as shown in the Appendix. The following study is devoted to solve the dispersion relation (2) in two different cases: one with a single hot electron distribution and another with both cold and hot electron components.

### III. INSTABILITIES WITH HOT PLASMAS

We solve the dispersion relation (2) by assuming that the electron distribution function is a constant within certain momentum space, which is called the waterbag model. This allows for great simplification in calculating the dispersion relation, which finally reduces to a polynomial equation. But one has to be reminded that this simplification by the waterbag model is brought at the price of losing the Landau damping, which occurs in Gaussian-like distribution function. In the waterbag model, the distribution function of the longitudinal momentum is

$$f(p) = [H(p - p_h) - H(p - p_l)]/\Delta p, \tag{4}$$

where $\Delta p = p_h - p_l$, $H(p)$ is the Heaviside step function, $p_h$ and $p_l$ are the high and low boundaries in momentum space, respectively. The dispersion relation for the driving wave is now $\omega_0^2 = k_0^2 c^2 + \omega_p^2 \langle \gamma^{-1} \rangle$, where $\langle \gamma^{-1} \rangle = (\Delta p)^{-1} \ln(\gamma + p)|_{p_l}^{p_h}$. In the following in this section, we only consider a waterbag distribution, which is symmetric about zero, i.e., $p_h = -p_l = p_m > 0$. In this case, we have $\gamma_m = (1 + a_0^2/2 + p_m^2)^{1/2}$, $\langle \gamma^{-1} \rangle = (2p_m)^{-1} \ln[(1 + v_m)/(1 - v_m)] \equiv \gamma_m'^{-1}$, and the temperature $T = \int dp (p^2/\gamma) f(p) = (2\Delta p)^{-1} [\gamma p - \gamma_a^2 \ln(\gamma + p)]|_{p_l}^{p_h} = (\gamma_m - \gamma_a^2 \gamma_m'^{-1})/2$ with $\gamma_a = (1 + a_0^2/2)^{1/2}$. From the dielectric function, we obtain the dispersion relation for the plasma wave

$$\omega^2 = \omega_p^2/\gamma_m + c^2 k^2 v_m^2 \equiv \omega_e^2, \tag{5}$$

where $v_m = p_m/\gamma_m$ is the maximum longitudinal velocity. When $p_m \ll \gamma_a$, $T \approx \gamma_a v_m^2/3$, one obtains $\omega_e^2 \approx (\omega_p^2 + 3Tc^2 k^2)/\gamma_a$.

For the SRS including the stimulated Raman backward scattering (SRBS) and the stimulated Raman forward scattering (SRFS), the plasma frequency and wave number can be obtained by substituting the dispersion relation of the plasma wave (5) into $D_{-1} = 0$ for three-wave resonance. Figure 1(a) is a graphic version of the three-wave resonance $k_0 = k + k_s$ and $\omega_0 = \omega + \omega_s$, where $\omega_s$ and $k_s$ are the frequency and wave number of the scattered waves, respectively. There are two interacting points between $\omega_e$ and $\omega = \omega_0 - [(k_0 - k)^2 c^2 + \omega_p^2/\gamma_m']^{1/2}$, corresponding to SRFS and SRBS, respectively. Figure 1(b) shows the wave vector $k$ as a function of the maximum velocity $v_m$. With the increase of the thermal velocities, the $k$ vector decreases for the SRBS branch and increases for the SRFS branch. For given plasma densities and laser intensities, there is an implicit cutoff thermal velocity (about $v_m = 0.6$ for $\omega_p = 0.4$ and $a_0 = 0.1$) at which SRFS and SFBS merge with each other. Both SRFS and SRBS disappear when $v_m$ is larger than this cutoff thermal velocity. This cutoff effect with the thermal velocity is similar to the cutoff of SRS with the plasma density since the plasma frequency is a function of both the plasma density and the thermal velocity.

With the symmetric waterbag distribution, the coupling function is

$$S = \frac{a_0^2}{4\gamma_m \gamma_a^2} \frac{\omega_p^2}{D_p} (k^2 c^2 + \omega_p^2/\gamma_m - \omega^2), \tag{6}$$

where $D_p = \omega^2 - c^2 k^2 v_m^2 - \omega_p^2/\gamma_m$. With Eqs. (2) and (6), the temporal growth rate for SRS and RMI can be found analytically at low plasma densities. We obtain the temporal growth rate [$\Gamma = \mathrm{Im}(\omega)$]

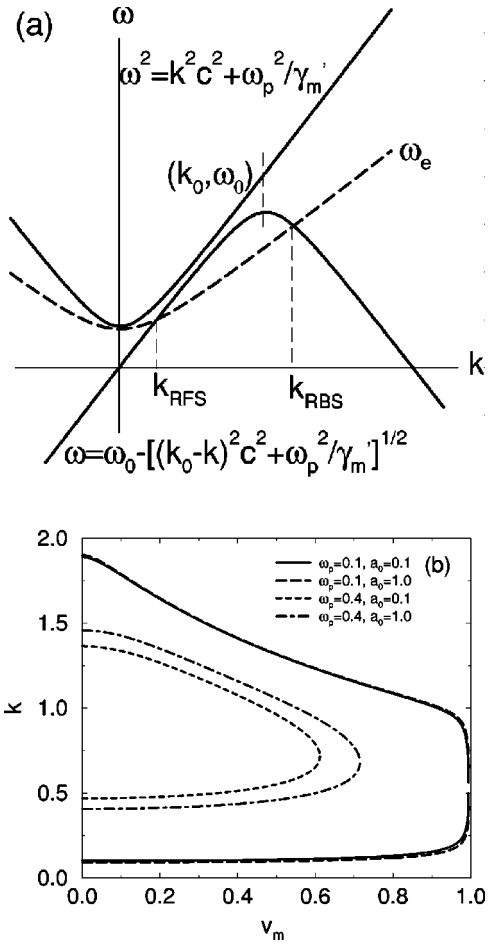


FIG. 1. (a) Frequency vs wave-number diagram illustrating the three-wave resonance of SRS; (b) wave vector of SRS as a function of the maximum velocity in the waterbag distribution of electrons for various densities and laser intensities. Here, $k$ is normalized by $\omega_0/c$ and $v_m$ by $c$.

$$\Gamma_{\mathrm{SRBS}}=\left(\frac{\omega_p^2\omega_0}{\omega_e}\right)^{1/2}\frac{a_0}{4\gamma_a^{3/2}\gamma_{0m}^{1/2}}, \tag{7}$$

for the SRBS around $kc\approx 2\omega_0/(1+v_m)$ and $\omega\approx\omega_e=[\omega_p^2/\gamma_m+4\omega_0^2v_m^2/(1+v_m)^2]^{1/2}$, where $\gamma_{0m}=1/(1-v_m^2)^{1/2}$. For SRFS, both the Stokes and anti-Stokes waves have to be considered. The growth rate is

$$\Gamma_{\mathrm{SRFS}}=\frac{\omega_p^2}{\omega_0}\frac{a_0}{\sqrt{8}\gamma_a^2\gamma_{0m}}, \tag{8}$$

at $kc\approx\omega\approx\omega_p(\gamma_{0m}/\gamma_a)^{1/2}$. Apparently, Eqs. (7) and (8) show that thermal temperatures tend to reduce the instability growth rate. The results for the cold plasma [3–5] are recovered when $v_m=0$. For RMI, assuming $\omega=c^2kk_0/\omega_0+\delta\omega$, we obtain

$$\delta\omega=\frac{kc}{2\gamma_m'}\frac{\omega_p^2}{\omega_0^2}\left[\frac{k^2c^2}{\omega_0^2}-\frac{a_0^2}{2\gamma_a^2\gamma_m\gamma_m'^{-1}}\frac{1+\gamma_m\gamma_m'^{-1}k^2c^2/\omega_0^2}{1-\gamma_m(k_0^2c^2/\omega_0^2-v_m^2)k^2c^2/\omega_p^2}\right]^{1/2}. \tag{9}$$

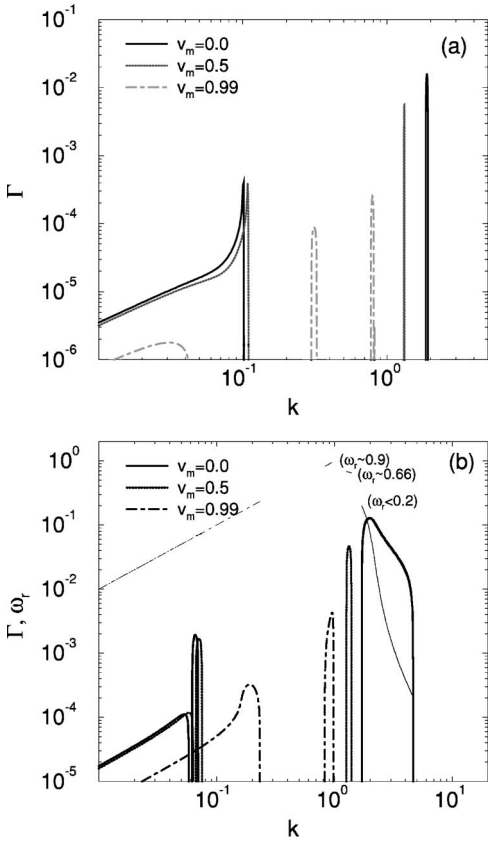


FIG. 2. Temporal growth rate for $\omega_p/\omega_0=0.1$ at various maximum velocities in the waterbag distribution for (a) $a_0=0.1$ and (b) $a_0=3.0$. The corresponding thin lines in (b) are the real part of $\omega$. Both $\Gamma$ and $\omega_r$ are normalized by $\omega_0$ and $k$ by $\omega_0/c$.

It shows that RMI occurs for $kc<\omega_p/[\gamma_m(k_0^2c^2/\omega_0^2-v_m^2)]^{1/2}\sim\omega_p(\gamma_{0m}/\gamma_a)^{1/2}$, i.e., it locates in a lower $k$-vector region than SRFS. Notice that the above formula cannot reduce to that given in [3] when setting $v_m=0$. The RMI growth rate given there is obtained by some simple substitutions using an expression derived for weakly relativistic intensities [7,8]. However, some approximations used to derive that expression are no longer valid at high-light intensities. Here we find Eq. (9) agrees with numerical results from the dispersion relation.

We solve the dispersion relation (2) numerically [26] together with Eq. (6). The resulting dispersion relation is a polynomial equation of degree eight. Figure 2 shows examples of the growth rate as a function of the wave vector when $\omega_p=0.1$. The $k$ vectors for SRS shift from the cold plasma theory in a way predicted in Fig. 1(b). The growth rates are reduced from the cold plasma theory when the thermal velocity is high as expected from Eqs. (7) and (8). In Fig. 2(b), the real part of the plasma wave frequency $\omega_r$ $[=\mathrm{Re}(\omega)]$ is also plotted. For SRBS, $\omega_r$ increases with the temperatures; as a result, the frequency of the scattered wave will decrease. For SRFS, since the $k$ vector increases with the temperatures, correspondingly $\omega_r$ increases as well. Another example is displayed in Fig. 3 for $\omega_p=0.4$. As shown in Fig. 3(a), near the cutoff velocity at $v_m=0.6$ when $a_0=0.1$, SRFS and SRBS merge in $k$ space. If $v_m>0.6$, both SRFS and SRBS disappear and only the RMI is found with a low growth rate, consistent with Fig. 1(b). When $a_0=1.0$, SRS

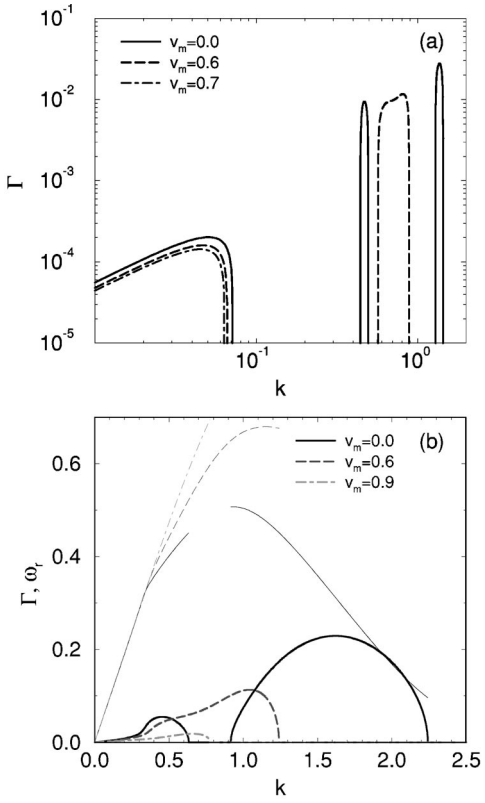


FIG. 3. Temporal growth rate for $\omega_p/\omega_0=0.4$ at various maximum velocities in the waterbag distribution for (a) $a_0=0.1$ and (b) $a_0=1.0$. The corresponding thin lines in (b) are the real part of $\omega$. Both $\Gamma$ and $\omega_r$ are normalized by $\omega_0$ and $k$ by $\omega_0/c$.

and RMI merge with each other. In this case, both the growth rate and the unstable region in $k$ vector can be reduced significantly by high temperatures, but there is no clear cutoff owing to the merging of SRS and RMI, as shown in Fig. 3(b). Thus, high temperatures are relatively easier to suppress SRS at low-light intensities than at high intensities. Similar to Fig. 2(b), the real frequency $\omega_r$ increases with the temperatures in this example.

## IV. INSTABILITIES WITH BOTH COLD AND HOT ELECTRON COMPONENTS

As mentioned in the Introduction, some PIC simulations show that part of the electrons are accelerated forward to very high energy by the intense lasers, while other parts of the electrons remain at low energy level. As a result, the electron distribution appears to have two different thermal temperatures: a relatively cold electron component and another with temperature up to several MeV. This kind of energy distribution may exist, for example, inside the relativistic self-focusing channel of a powerful laser beam, where the forward acceleration of electrons is often accompanied by cold electrons flowing inwards from surrounding regions due to induced electrostatic fields. In this section, we make an attempt to study the effect of such kinds of electron distributions on parametric instabilities. For simplicity, we consider the following distribution function

$$f(p)=n_1\delta(p)+n_2[H(p-p_h)-H(p-p_l)]/\Delta p, \quad (10)$$

where $\delta(p)$ is the delta function, $n_1$ and $n_2$ represent the relative density ratio between the cold electron component and the hot tail, respectively, and $n_1+n_2=1$. For this distribution function, there is a net current generating a static magnetic field. The estimated condition given in Sec. II for neglecting this magnetic field applies here, which now requires $(\omega_p/\omega_0)^2<1/3n_2$. Also for distribution function (10), the dispersion relation of the driving wave is $\omega_0^2=k_0^2c^2+\omega_p^2\langle\gamma^{-1}\rangle$ with $\langle\gamma^{-1}\rangle=n_1/\gamma_a+n_2(\Delta p)^{-1}\ln[(\gamma_h+p_h)/(\gamma_l+p_l)]$; the dielectric function is given by

$$\epsilon=1-\omega_p^2\left[\frac{n_1/\gamma_a}{\omega^2}+\frac{n_2/\gamma_T}{(\omega-ckv_h)(\omega-ckv_l)}\right], \quad (11)$$

where $v_h=p_h/\gamma_h$, $v_l=p_l/\gamma_l$, $\gamma_h=(1+a_0^2/2+p_h^2)^{1/2}$, $\gamma_l=(1+a_0^2/2+p_l)^2$, and $\gamma_T^{-1}=\Delta v/\Delta p$ with $\Delta v=v_h-v_l$. From Eq. (11) with $v_l=0$ one sees immediately that at high wave numbers one has either a phase velocity nearly equal to $cv_h$ or a frequency given by the cold plasma frequency $\omega_p(n_1/\gamma_a)^{1/2}$. At low wave numbers one has the usual total plasma frequency with both hot and cold components, together with a curious low-frequency acousticlike wave resulting from the hot electron screening of the cold plasma oscillations. The coupling function is as follows:

$$S=\frac{a_0^2\omega_p^2}{4}\left\{\frac{\omega_p^2}{c^2k^2\epsilon}\left[\frac{n_1}{\gamma_a^2}\frac{c^2k^2}{\omega^2}+\frac{n_2}{\gamma_h\gamma_l\Delta p}\frac{(\Delta pkc-\Delta\gamma\omega)kc}{(\omega-ckv_h)(\omega-ckv_l)}\right]^2-\frac{\omega^2-k^2c^2}{\gamma_a^2}\left[\frac{n_1}{\gamma_a\omega^2}+\frac{n_2}{\gamma_T(\omega-ckv_h)(\omega-ckv_l)}\right]\right\}, \quad (12)$$

where $\Delta\gamma=\gamma_h-\gamma_l$. In the following, we consider $v_l=0$ only, corresponding to zero gap between cold electrons and the hot tail. We assume that $p_h>0$, i.e., the hot tail copropagates with the laser. Let us first consider the wave vector as a function of the high velocity of the hot tail $v_h$. The three-wave resonance constructed in the same way as in Fig. 1(a) is illustrated in Fig. 4(a). There are six intersecting points between $\epsilon=0$ and $\omega=\omega_0-[(k_0-k)^2c^2+\omega_p^2\langle\gamma^{-1}\rangle]^{1/2}$. Since both the frequency and wave vector of the plasma wave only take positive values, there are actually three matching points, two SRBS branches for the cold electron component and the hot tail, respectively, and a mixed SRFS branch located at low $k$-vector value. Figure 4(b) shows the $k$ vectors of these three branches as a function of the high velocity of the hot tail obtained from the three-wave resonace by $\epsilon=0$ and $D_{-1}=0$. The $k$ vectors change with the density ratio $n_1/n_2$. If there is not a hot tail, it is just the cold plasma result; if there is no cold plasma, the velocity dependence looks similar to Fig. 1(b) for hot plasma with symmetric waterbag distribution; if both components exist, it is a mixture of the last two cases, resulting in three branches of SRS. Both the frequency and wave vector of SRFS and the hot-tail branch of SRBS change with the high velocity, while those of the cold plasma branch of SRBS do not change with it. Therefore, as the high velocity increases, the thermal cut-

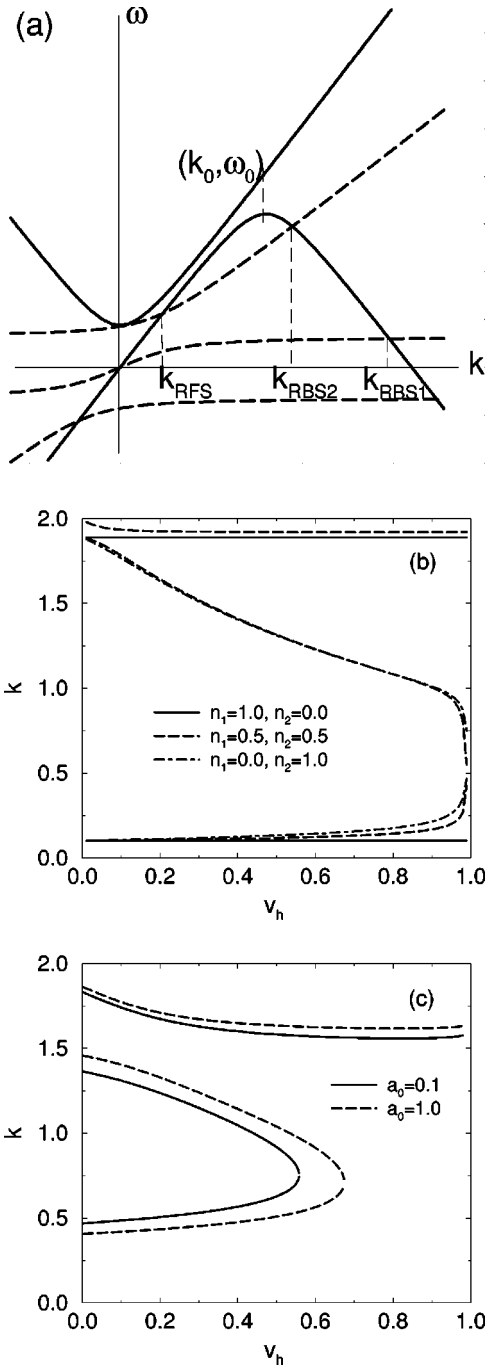


FIG. 4. (a) Frequency vs wave-number diagram illustrating the three-wave resonance of SRS for electrons with both a cold component and a hot tail, where $k_{RBS1}$ and $k_{RBS2}$ correspond to the cold and hot branches of SRBS, respectively; (b) wave vector of SRS as a function of the high velocity of the hot tail for different density ratio between the cold and hot components for $\omega_p=0.1$ and $a_0=0.1$; (c) wave vector of SRS as a function of the high velocity of the hot tail for $\omega_p=0.4$ and $n_1=n_2=0.5$. Here, $k$ is normalized by $\omega_0/c$ and $v_m$ by $c$.

off effect found for the hot plasma in the last section appears only for the hot tail branch of SRBS and SRFS, as shown in Fig. 4(c).

In the case $v_l=0$, the resulting dispersion relation is a polynomial equation of degree ten, which has to be solved numerically. Before presenting the results, we should mention that the dielectric function (11) may also invlove the two stream instability. To study the condition for this instability, we notice that $\epsilon=0$ reduces to $\hat{\omega}^3-\hat{k}v_h\hat{\omega}^2-(n_1/\gamma_a+n_2/\gamma_T)\hat{\omega}+\hat{k}v_h n_1/\gamma_a=0$, where $\hat{\omega}=\omega/\omega_p$ and $\hat{k}=kc/\omega_p$. There are imaginary roots for this cubic equation only when $d=4\hat{k}^4v_h^4 n_1/\gamma_a+18\hat{k}^2v_h^2[n_1n_2/\gamma_a\gamma_T+(n_1/\gamma_a+n_2/\gamma_T)^2/18-n_1^2/2\gamma_a^2]+4(n_1/\gamma_a+n_2/\gamma_T)^3<0$. This implies that at least it must satisfy $n_1n_2/\gamma_a\gamma_T+(n_1/\gamma_a+n_2/\gamma_T)^2/18-n_1^2/2\gamma_a^2<0$, or $n_2\gamma_a/n_1\gamma_T<0.4$. Actually, the two stream instability occurs in more limited parameter regimes. Therefore, in the following we only present results for parameters when this instability does not exist.

Examples of numerical results of the dispersion relation are displayed in Fig. 5 for some plasma densities, light intensities, and the high velocities of the hot tail. For a given high velocity, Fig. 5(a) shows that there are actually two SRBS branches, one for cold electrons and another for the hot tail. As the high velocity of the hot tail increases, the growth rate of the hot-tail branch of SRBS decreases; it also shifts to a low $k$ vector and SRFS shifts to a high $k$ vector, as expected from Fig. 4(b). On the other hand, both the growth rate and the $k$ vector of the cold plasma branch of SRBS do not depend on the high velocity. As shown in Figs. 5(a) and 5(b), the growth rate curves of the cold plasma branch (indicated by RBS1) for $v_h=0.5$ and 0.9 are overlapped. At the same density level ($n_1\sim n_2$), the cold plasma branch normally has a higher growth rate than the hot-tail branch. The hot-tail branch may have a higher growth rate than the cold plasma branch only when the electron density of the hot tail is much higher than the cold plasma, as shown in Fig. 5(c). The real frequency $\omega_r$ of the hot-tail branch, which increases with the high velocity, is normally higher than the cold plasma branch when $n_1\sim n_2$. The thermal cutoff feature is easily seen at relatively high plasma densities. Calculation verifies that the hot-tail branch of SRBS merges with SRFS in $k$-vector space at $v_h=0.5$ at low light intensities $a_0=0.1$ and $n_1=n_2=0.5$, for example. If $v_h$ takes higher values, they disappear and only the RFI and the cold plasma branch of SRBS are left. This thermal cutoff feature with the hot tail is just similar to a hot plasma shown in Fig. 3(a). At high light intensities as shown in Fig. 5(d), owing to the merging of the hot-tail branch of SRBS with SRFS and RFI, there is not a clear cutoff hight velocity. The merged hybrid instability can be significantly suppressed when the hot tail extends to a sufficient high-energy level of a few MeV. On the other hand, the cold plasma branch of SRBS is not very sensitive to the high-energy tail. But one can see the increase of its growth rate with the hot-tail velocity, in contrast to the hot-tail branch of SRBS and SRFS. When the hot-tail velocity approaches the velocity of light, the result for purely cold plasma is recovered. Thus one expects that the cold plasma branch of SRBS will become dominant when the hot tail extends to very high energy, even if the electron density of the cold component is much lower than the hot tail.

## V. SUMMARY AND DISCUSSIONS

We have studied the SRS and RMI instabilities of intense lasers in plasma with relativistic hot electrons by use of the waterbag model on the distribution function of electrons. In

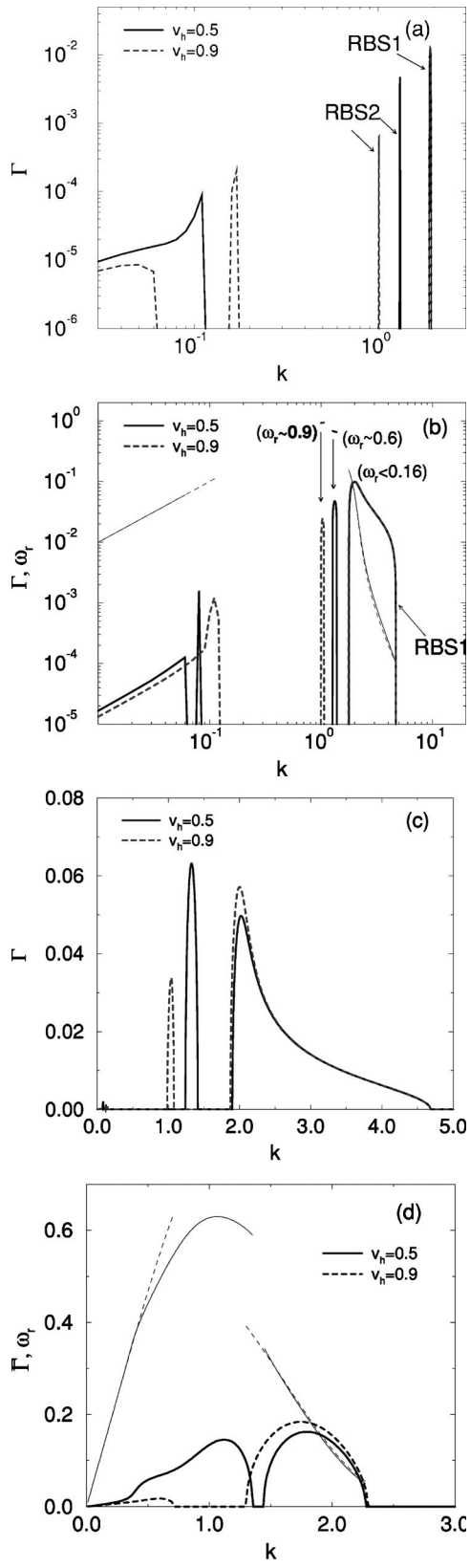


FIG. 5. Temporal growth rate at various high velocities of the hot tail. (a) $\omega_p/\omega_0=0.1$, $a_0=0.1$, and $n_1=n_2=0.5$; (b) $\omega_p/\omega_0=0.1$, $a_0=3.0$, and $n_1=n_2=0.5$; (c) $\omega_p/\omega_0=0.1$, $a_0=3.0$, $n_1=0.1$, and $n_2=0.9$; (d) $\omega_p/\omega_0=0.4$, $a_0=1.0$, and $n_1=n_2=0.5$. The corresponding thin lines in (b) and (d) are the real part of $\omega$. Both $\Gamma$ and $\omega_r$ are normalized by $\omega_0$ and $k$ by $\omega_0/c$. Notice that the cold branches of SRBS for $v_h=0.5$ and 0.9 (indicated by RBS1) are overlapped in (a) and (b).

the case with a single hot electron distribution, the temporal growth rates of the instabilities are given analytically for low plasma densities and numerically for various parameters. Due to high temperatures, the growth rate reduces significantly from the cold plasma results. High temperatures also shift the positions of the wave vectors and enhance the frequencies of the excited plasma waves, and therefore reduce the frequencies of the scattered SRFS and SRBS waves. At low light intensities, there exists a cutoff thermal velocity for a given plasma density, beyond which SRS disappears. At high light intensities, the SRS and RMI merge with each other. As a result, there is not a clear cutoff thermal velocity. But high temperatures can still significantly suppress the merged hybrid instability by reducing the growth rate and suppressing the unstable region in wave-vector space.

In the case with both a cold electron component and a high-energy tail copropagating with the lasers, there appear a SRFS branch and two SRBS branches; one corresponds to the cold plasma component and another to the hot tail. The effects of the hot-tail velocity on the hot-tail branch of SRBS and the SRFS are similar to a high temperature, which leads to the reduced growth rate and/or the cutoff of SRS above certain velocity of the hot tail, while the cold plasma branch remains insensitive to the hot tail. When the hot tail extends to sufficiently high energy so that the corresponding SRBS and SRFS are significantly suppressed, the behavior of laser pulse propagation will be dominated by the cold electron component in the present one-dimensional calculation.

The calculation in Sec. IV for distributions with both cold and hot components of electrons demonstrates that cold electrons even at much smaller densities than hot electrons can play a dominant role in the excitation of parametric instabilities. In real experiments, the electron distributions may look much smoother than used in this paper. In this situation, it is not clear if there would arise distinct cold and hot unstable modes at the same time. This is the object of future work by using a smooth distribution, which would also include Landau damping and additional instability such as the stimulated Compton scattering [27]. In addition, we note that present work is valid in one-dimensional geometry. Two-dimensional geometry would allow for other instabilities such as filamentation instability of both electron beams and laser beams and Weibel instability of electron beams, which are coupled with each other, and are more complicated than the present one-dimensional parametric instabilities. But the waterbag model may also serve as a tool to simplify the calculation without losing the main physics.

## ACKNOWLEDGMENT

One of the authors (Z.M.S.) acknowledges the support of the Japan Society for the Promotion of Science.

## APPENDIX: DISPERSION RELATIONS EQS. (1) AND (2)

The dispersion relation of a relativistic plane wave in cold, not moving plasma is well known [28]. Here, we derive the dispersion relation in plasma with components of electrons moving with different velocities. Instead of starting with the Vlasov equation for electrons, we consider the distribution function of electrons as an assembly of cold elec-

tron beams with different velocities and start with the following sets of equations describing both the laser fields and electron motions:

$$\frac{1}{c^2}\frac{\partial^2 \mathbf{a}}{\partial t^2}-\nabla^2\mathbf{a}=-\frac{1}{c}\frac{\partial}{\partial t}\nabla\phi-\frac{\omega_p^2}{c^2}\sum_j \frac{n_j}{\gamma_j}\mathbf{p}_j, \tag{A1}$$

$$\frac{\partial \mathbf{p}_j}{\partial t}=\frac{\partial \mathbf{a}}{\partial t}+c\nabla(\phi-\gamma_j)+c\mathbf{v}_j\times\nabla\times(\mathbf{p}_j-\mathbf{a}), \tag{A2}$$

$$\frac{\partial n_j}{\partial t}+c\nabla\cdot\left(\frac{n_j\mathbf{p}_j}{\gamma_j}\right)=0, \tag{A3}$$

$$\nabla^2\phi=\frac{\omega_p^2}{c^2}\left(\sum_j n_j-1\right), \tag{A4}$$

where $\mathbf{a}$ and $\phi$ are, respectively, the vector and scalar potentials normalized by $mc^2/e$, $\mathbf{p}_j$ is the electron momentum normalized by $mc$, $j=1,2,\ldots$ denotes different cold beams of electrons moving at different velocities, $n_j$ is the density of the $j$ component of electrons normalized by the unperturbed density $N_0=\Sigma_j N_{0j}$, and $\omega_p^2=4\pi N_0 e^2/m$ is the electron plasma frequency, $n_j=N_{0j}/N_0$. The Coloumb gauge $\nabla\cdot\mathbf{a}=0$ has been used. We first derive the dispersion relation (1).

In homogeneous plasmas, assuming the plane wave propagates with the comoving coordinate $\tau=t-x/u$, we obtain from Eq. (A2)

$$\mathbf{p}_{j,\perp}=\mathbf{a}, \tag{A5}$$

$$\beta p_{j,x}+\phi-\gamma_j=K_j, \tag{A6}$$

where $K_j=\beta p_{j0}-\gamma_{j0}$ is a constant depending on the initial conditions of electron component $j$, and $\beta=u/c$. From these constants of integration, one finds

$$p_{j,x}=\gamma_\beta^2[-\beta\phi_j+\sqrt{\phi_j^2+\gamma_\beta^{-2}(1+a^2/2)}], \tag{A7}$$

$$\gamma_j=\gamma_\beta^2[-\phi_j+\beta\sqrt{\phi_j^2+\gamma_\beta^{-2}(1+a^2/2)}], \tag{A8}$$

where $\gamma_\beta=(\beta^2-1)^{1/2}$ and $\phi_j=\phi-K_j$. From Eq. (A3), one obtains

$$n_j=\frac{\beta-v_{j0}}{\beta-v_{jx}}n_{j0}. \tag{A9}$$

Notice that here the zero subscripts such as $p_{j0}$, $\gamma_{j0}$, $v_{j0}$, and $n_{j0}$ denote the corresponding quantities before the interaction with the laser. Substituting these into Eqs. (A1) and (A4),

$$\frac{\partial^2}{\partial\tau^2}a=-\frac{\beta^2}{\beta^2-1}\left(\omega_p^2\sum_j\frac{n_j}{\gamma_j}\right)a+\frac{\beta}{\beta^2-1}\frac{\partial^2}{\partial\tau^2}\phi, \tag{A10}$$

$$\frac{\partial^2}{\partial\tau^2}\phi=\beta^2\omega_p^2\sum_j(n_j-n_{j0}). \tag{A11}$$

One can always find appropriate constant value of $\phi$, so that $\Sigma_j(n_j-n_{j0})=0$, i.e.,

$$\sum_j[1-\beta v_{j0}-(\beta-v_{j0})\phi_j/\sqrt{\phi_j^2+\gamma_\beta^{-2}(1+a^2/2)}]n_{j0}=0.$$

In the case of a single-electron beam, for example, dropping the subscript $j$, we find $\phi=(1-\beta v_0)\gamma_a\gamma_0+K$, $p_x=\gamma_a\gamma_0 v_0$ and $\gamma=\gamma_a\gamma_0$, where $\gamma_a=(1+a^2/2)^{1/2}$ and $\gamma_0=(1-v_0^2)^{-1/2}$. In this case, there is no charge separation. Therefore the following dispersion relation is readily obtained from Eq. (A10):

$$\omega_0^2=\omega_p^2\beta^2/(\beta^2-1)\sum_j(n_j/\gamma_j), \tag{A12}$$

which is just $\omega_0^2=k_0^2c^2+\omega_p^2\Sigma_j(n_j/\gamma_j)$ or Eq. (1). This dispersion relation is purely electromagnetic and may occur only when the electron beams interact with a semi-infinite laser pulse with sufficient long leading front, thereby avoiding plasma wave excitation.

Next, we derive the dispersion relation (2). We perturb Eqs. (A1)–(A4) with the perturbation quantities $\tilde{\mathbf{a}}$, $\tilde{\mathbf{p}}_j$, $\tilde{n}_j$, and $\tilde{\phi}$, and expand them in the form of $\tilde{g}=\Sigma_{m=-\infty}^{+\infty}\tilde{g}_m\exp[i(\theta+m\theta_0)]$, with $\theta_0=\mathbf{k}_0\cdot\mathbf{x}-\omega_0 t$ and $\theta=\mathbf{k}\cdot\mathbf{x}-\omega t$. For one-dimensional perturbation where the perturbation wave vector is along the propagation direction of the driving wave, i.e., $\mathbf{k}=k\mathbf{e}_x$, following routine calculations, we obtain a dispersion relation

$$D_{m+1}D_{m-1}-(D_{m+1}+D_{m-1})\omega_p^2\sum_j d_{j,m}=0, \tag{A13}$$

where $D_m=\omega_m^2-c^2k_m^2-\omega_p^2\Sigma_j(n_j/\gamma_j)$, $\omega_{j,m}=\omega_m-ck_m v_{j0}$, $v_{j0}=p_{j0}/\gamma_j$, $\omega_m=\omega+m\omega_0$, $\mathbf{k}_m=\mathbf{k}+mk_0\mathbf{e}_x$, and

$$d_{j,m}=\left(\frac{a_0}{2}\right)^2\frac{n_j}{\gamma_j^3}\left\{\frac{c^2k_m^2}{\omega_{j,m}^2}\Gamma_{j,m}\left[1+\frac{\gamma_j}{\epsilon_m}\sum_l\left(\frac{\omega_p^2}{\omega_{l,m}^2}\frac{n_l}{\gamma_l^2}\Gamma_{l,m}\right)\right]-\frac{\omega_m}{\omega_{j,m}}\right\}, \tag{A14}$$

with $\epsilon_m=1-\Sigma_j(\omega_p^2 n_j)/(\omega_{j,m}^2\gamma_j\gamma_{j0}^2)$, $\gamma_{j0}^2=1/(1-v_{j0}^2)=\gamma_j^2/\gamma_a^2$, $\gamma_a=(1+a_0^2/2)^{1/2}$, $\Gamma_{j,m}=1-\omega_m v_{j0}/ck_m$. Here, after Eq. (A13), the zero subscripts such as $p_{j0}$, $\gamma_{j0}$, and $v_{j0}$ denote the unperturbed value in the presence of the laser. One notices that $\epsilon_m=0$ can be used to study the plasma wave with multicomponents of electrons moving with different velocities [25]. In Eq. (A13), $m$ can be an arbitrary integer. It shows that there is no coupling between different harmonics when the driving wave is circularly polarized. Since there is no harmonics generation in the driving wave, one should take $m=0$ in this dispersion relation. Thus, one obtains Eq. (2) with the coupling function $S=\omega_p^2\Sigma_j d_{j,0}$. The latter can be rewritten as

$$S=\frac{a_0^2\omega_p^2}{4}\left\{\frac{c^2k^2\omega_p^2}{\epsilon_0}\left(\sum_j \frac{n_j\Gamma_{j,0}}{\gamma_j^2\omega_{j,0}^2}\right)^2-(\omega^2-c^2k^2)\sum_j \frac{n_j}{\gamma_j^3\omega_{j,0}^2}\right\}. \tag{A15}$$

This is an extension to the dispersion for SRS and RMI as given in Refs. [3–5] to include the drift motion of electrons. If substituting the sum with integral, one can verify that Eq. (A15) is equivalent to Eq. (3).


[1] W. L. Kruer, *The Physics of Laser Plasma Interaction* (Addison-Wesley, New York, 1988), and references therein.

[2] J. F. Drake, P. K. Kaw, Y. C. Lee, G. Schmidt, C. S. Liu, and M. Rosenbluth, Phys. Fluids **17**, 778 (1974); D. W. Forslund, J. M. Kindel, and E. Lindman, *ibid.* **18**, 1002 (1975); K. Estabrook and W. L. Kruer, *ibid.* **26**, 1892 (1983).

[3] C. D. Decker *et al.*, Phys. Plasmas **3**, 2047 (1996).

[4] A. S. Sakharov and V. I. Kirsanov, Phys. Rev. E **49**, 3274 (1994); A. S. Sakharov *et al.*, Plasma Phys. Rep. **21**, 587 (1995).

[5] S. Guerin, G. Laval, P. Mora, J. C. Adam, and A. Heron, Phys. Plasmas **2**, 2807 (1995).

[6] B. Quesnel, P. Mora, J. C. Adam, A. Heron, and A. Laval, Phys. Plasmas **4**, 3358 (1997).

[7] C. E. Max, J. Aron, and A. B. Langdon, Phys. Rev. Lett. **33**, 209 (1974).

[8] C. J. Mckinstrie and R. Bingham, Phys. Fluids B **4**, 2626 (1992).

[9] T. M. Antonsen, Jr. and P. Mora, Phys. Fluids B **5**, 1440 (1993).

[10] W. B. Mori, C. D. Decker, D. E. Hinkel, and T. Katsouleas, Phys. Rev. Lett. **72**, 1482 (1994); C. D. Decker, W. B. Mori, and T. Katsouleas, Phys. Rev. E **50**, R3338 (1994).

[11] H. C. Barr, S. J. Berwick, and P. Mason, Phys. Rev. Lett. **81**, 2910 (1998).

[12] M. Tabak *et al.*, Phys. Plasmas **1**, 1626 (1994).

[13] S. C. Wilks *et al.*, Phys. Rev. Lett. **69**, 1383 (1992).

[14] A. Pukhov and J. Meyer-ter-Vehn, Phys. Rev. Lett. **76**, 3975 (1996); **79**, 2686 (1997); Phys. Plasmas **5**, 1880 (1998); A. Pukhov, Z.-M. Sheng, and J. Meyer-ter-Vehn, *ibid.* **6**, 2847 (1999).

[15] J. C. Adam *et al.*, Phys. Rev. Lett. **78**, 4765 (1997).

[16] K. C. Tzeng and W. B. Mori, Phys. Rev. Lett. **81**, 104 (1998).

[17] Y. Sentou, K. Mima, T. Taguchi, S. Miyamoto, and Y. Kishimoto, Phys. Plasmas **5**, 4366 (1998).

[18] B. F. Lasinski *et al.*, Phys. Plasmas **6**, 2041 (1999).

[19] R. Kodama *et al.*, Phys. Rev. Lett. **77**, 4906 (1996).

[20] M. Borghesi *et al.*, Phys. Rev. Lett. **78**, 879 (1997); **81**, 112 (1998).

[21] G. Malk *et al.*, Phys. Rev. Lett. **79**, 2053 (1997).

[22] J. Fuchs *et al.*, Phys. Plasmas **6**, 2563 (1999); **6**, 2569 (1999).

[23] M. H. Key *et al.*, Phys. Plasmas **5**, 1966 (1998).

[24] J. Arons, C. A. Norman, and C. E. Max, Phys. Fluids **20**, 1302 (1977).

[25] C. J. Mckinstrie and D. F. Dubois, Phys. Fluids **31**, 278 (1988).

[26] W. H. Press, S. A. Teukolsky, W. T. Vetterling, and B. P. Flannery, *Numerical Recipes in Fortran* (Cambridge University Press, New York, 1992), Chap. 9.

[27] A. T. Lin and J. M. Dawson, Phys. Fluids **18**, 201 (1975).

[28] A. I. Akhiezer and R. V. Polovin, Zh. Éksp. Teor. Fiz. **30**, 915 (1956) [ Sov. Phys. JETP **3**, 696 (1956)].